Progress In Electromagnetics Research C, Vol. 132, 37–49, 2023

Propagation of Electromagnetic Waves along a Compact Nerve Fiber in the Optical and Infrared Ranges

Vasiliy A. Es'kin*, Sergey V. Leonov, Oleg M. Ostafiychuk, and Alexander V. Kudrin

Abstract—A study is made of the guiding properties of a nerve fiber consisting of myelinated axons as applied to electromagnetic waves in the optical and infrared ranges. Using a rigorous representation of the electromagnetic field in the presence of a nerve fiber, the dispersion characteristics and field distributions of modes guided by the fiber are analyzed for different values of the dielectric permittivity of myelin. It is found that such a complex waveguide of natural origin is capable of supporting the propagation of weakly attenuated modes in the indicated ranges. It is shown that the dispersion properties and field structures of the modes of the nerve fiber can differ significantly from those of a single axon.

1. INTRODUCTION

Recent advances in biocompatible materials and neural technology have made it possible to create unique high-bandwidth brain-machine interface systems with an unprecedented packing density of electrodes [1, 2] and machine-brain devices that can serve as a prosthesis for human sensing systems [3]. In these applications, the excitation of electrophysiological activity in nerve cells is performed by a contact method due to the applied potential difference to the electrodes immersed in the nerve tissue. Such a method of nerve cell excitation has a number of disadvantages, including low resolution of excitation even by a relatively small single electrode due to the possible simultaneous stimulation of several closely spaced neurons. In addition, placing the electrodes in living tissue results in impairment of its integrity and normal function. Moreover, the body defense system can trigger an immune response and allergic reaction if the tissue has been in direct contact with a foreign body (electrode) for an extended period of time. The contactless methods of the nerve cell excitation by electromagnetic waves, which have been intensely developed in recent years [4–14], are free of such drawbacks. However, they require increased selectivity of stimulation of nerve tissue, which makes it necessary to solve the problem of the point (localized) action of an electromagnetic field excited by the system of sources on the nerve fiber. During such a stimulation, the inner part of a single nerve element (axon) may be heated to a greater or lesser extent, depending on the intensity of the applied field. Heating causes changes in the properties of nerve fibers and consequently affects the conditions for excitation or blockage of the nerve impulse (known as the action potential or depolarization wave) that propagates from the heated part of the nerve [8, 9]. This mechanism, currently discussed in the literature [9, 15], is related to changes in the electrical capacitance of the cell membrane during local heating by an electromagnetic field.

Recently, it has been shown that filamentary electromagnetic sources can produce a field that is localized in the individual elements of a compact nerve fiber [16] or a relatively large nerve [17] composed of myelinated axons. To improve the excitation efficiency of electrophysiological activity in individual axons by electromagnetic sources, it is important to know how localized electromagnetic

Received 19 February 2023, Accepted 27 March 2023, Scheduled 11 April 2023
* Corresponding author: Vasiliy A. Es'kin (vasiliy.eskin@gmail.com).
The authors are with the Department of Radiophysics, University of Nizhny Novgorod, 23 Gagarin Avenue, Nizhny Novgorod 603022, Russia.

waves propagate along the nerve fiber. Analyses of the dispersion properties of eigenmodes supported by a single axon were made in the cases where a myelin sheath was present [18–21] or absent [22, 23] on the surface of the axon. Transmission of electromagnetic signals by a single axon in the terahertz and infrared ranges was also studied, both in the presence and absence of a propagating electrical nerve impulse [19–23]. It is obvious that the presence of multiple axons in a nerve fiber can significantly affect the dispersion properties and field structures of electromagnetic waves guided by the nerve compared to those of a single axon. We note that the guided electromagnetic waves can play an important role in the process of a cell-to-cell communication, along with the well-known electrochemical signals [18, 19]. Despite the importance of this problem, we are not aware of any works that provide a rigorous electromagnetic approach to studying the properties of eigenmodes guided by a nerve fiber consisting of multiple myelinated axons.

It is the purpose of this work to study the propagation of electromagnetic waves in the optical and infrared ranges along a compact nerve fiber consisting of several axially homogeneous myelinated axons.

Our article is organized as follows. In Section 2, we formulate the problem and give the theoretical background. In Section 3, we discuss the propagation of eigenmodes along a nerve fiber and compare the dispersion properties of the modes of such a nerve with those of waves guided by a single axon. Section 4 presents the field structures of eigenmodes guided by a nerve fiber and a single axon. Finally, in Section 5, we draw our conclusions and present suggestions for future work. Some auxiliary mathematical expressions are given in the appendix.

2. FORMULATION OF THE PROBLEM AND BASIC EQUATIONS

Consider a nerve fiber consisting of tightly packed, parallel identical myelinated axons. We represent each axon as an infinitely long cylinder with the inner region of radius a_1 and the region filled with myelin (myelin sheath), which is located between cylindrical surfaces with the radii a_1 and a_2 ($a_1 < a_2$), as shown in Fig. 1(a). It is assumed that the myelin sheath is axially uniform. Such an assumption is acceptable because of the very small lengths of unmyelinated segments (nodes of Ranvier) of a real axon compared to the lengths of myelinated segments. All axons are immersed in a homogeneous outer medium. Let the relative dielectric permittivities of the outer and inner regions of each axon be equal to ε_1 and ε_3, respectively. Since these regions are predominantly filled with water, we can put $\varepsilon_1 = \varepsilon_3 = \varepsilon_w$, where ε_w is the complex dielectric permittivity of water, which can be obtained from the experimental data [24]. The myelin sheath is considered as a continuous medium with the effective relative dielectric permittivity ε_2, which can be written as (see [16, 25, 26] for details)

$$\varepsilon_2 = \left[\varepsilon_w(D_I + D_O) + 2\varepsilon_{lc}D_B + \varepsilon_p D_p\right]/D_\Sigma. \tag{1}$$

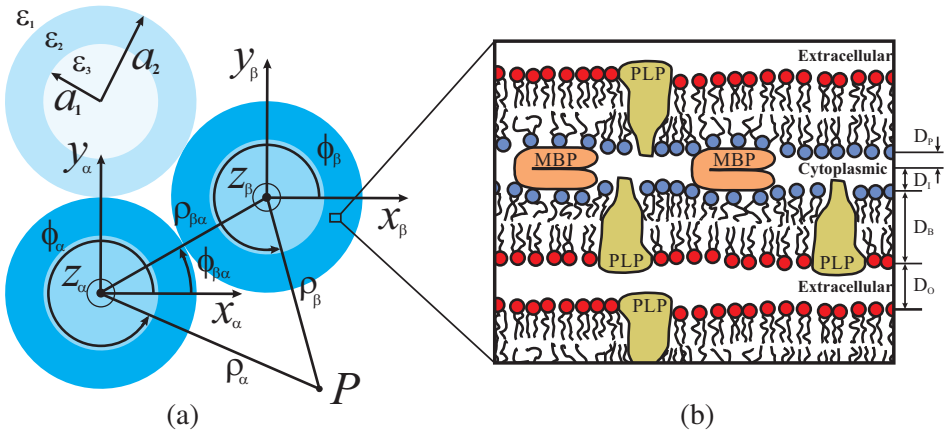

Figure 1. (a) Geometry of the problem and (b) the structure of the bilayer membranes of the myelin sheath according to [25].

Here, $\varepsilon_{\rm lc}$ is the dielectric permittivity of a medium consisting of proteolipid proteins (PLPs) and lipids; $\varepsilon_{\rm p}$ is the dielectric permittivity of myelin basic protein (MBP); $D_{\rm I}$ is the cytoplasm thickness; $D_{\rm O}$ is the thickness of the extracellular water gap; $D_{\rm B}$ is the thickness of the lipid bilayer; $D_{\rm p}$ is the effective protein thickness, and $D_\Sigma = 2D_{\rm B} + D_{\rm p} + D_{\rm I} + D_{\rm O}$ [see Fig. 1(b)]. Magnetic permeabilities of the considered media are equal to that of free space.

In a medium with the relative dielectric permittivity ε, the time-harmonic Maxwell equations for an electromagnetic field, with $\exp(i\omega t)$ time dependence dropped, have the form

$$\nabla \times \mathbf{E} = -i\omega\mu_0\mathbf{H}, \quad \nabla \times \mathbf{H} = i\omega\epsilon_0\varepsilon\mathbf{E}, \tag{2}$$

where ϵ_0 and μ_0 are the permittivity and permeability of free space, respectively. Let the symbol α denote the individual axon, so that we can introduce a cylindrical coordinate system $(\rho_\alpha, \phi_\alpha, z_\alpha)$ for the αth axon. Then the longitudinal components of the wave field in the coordinate system of the αth axon can be represented in terms of azimuthal harmonics as

$$\begin{bmatrix} E_{z;\alpha}(\mathbf{r}_\alpha) \\ H_{z;\alpha}(\mathbf{r}_\alpha) \end{bmatrix} = \sum_{m=-\infty}^{\infty} \begin{bmatrix} E_{z;\alpha,m}(\rho_\alpha, p) \\ H_{z;\alpha,m}(\rho_\alpha, p) \end{bmatrix} \exp(-im\phi_\alpha - ik_0 pz), \tag{3}$$

where m is the azimuthal index ($m = 0, \pm1, \pm2, \dots$), k_0 the free-space wave number, and p the normalized (to k_0) longitudinal wave number. The functions $E_{z;\alpha,m}(\rho_\alpha, p)$ and $H_{z;\alpha,m}(\rho_\alpha, p)$ satisfy the equations

$$\hat{L}_{\alpha,m} E_{z;\alpha,m}{=}0, \quad \hat{L}_{\alpha,m} H_{z;\alpha,m}{=}0, \tag{4}$$

where

$$\hat{L}_{\alpha,m} = \frac{\partial^2}{\partial\rho_\alpha^2} + \frac{1}{\rho_\alpha}\frac{\partial}{\partial\rho_\alpha} - \frac{m^2}{\rho_\alpha^2} + k_0^2 q_k^2, \quad k = 1, 2, 3,$$

and $q_k = \left(\varepsilon_k - p^2\right)^{1/2}$ denotes the transverse wave number in the kth region of the axon. The radial and azimuthal components of the electric and magnetic fields can be expressed via the longitudinal components as

$$\begin{aligned} E_{\rho;\alpha,m} &= -A\left(ip\frac{\partial E_{z;\alpha,m}}{\partial\rho_\alpha} + Z_0\frac{m}{\rho_\alpha}H_{z;\alpha,m}\right), \quad E_{\phi;\alpha,m} = A\left(iZ_0\frac{\partial H_{z;\alpha,m}}{\partial\rho_\alpha} - p\frac{m}{\rho_\alpha}E_{z;\alpha,m}\right), \\ H_{\rho;\alpha,m} &= -A\left(ip\frac{\partial H_{z;\alpha,m}}{\partial\rho_\alpha} - \varepsilon_k Z_0^{-1}\frac{m}{\rho_\alpha}E_{z;\alpha,m}\right), \quad H_{\phi;\alpha,m} = -A\left(i\varepsilon_k Z_0^{-1}\frac{\partial E_{z;\alpha,m}}{\partial\rho_\alpha} + p\frac{m}{\rho_\alpha}H_{z;\alpha,m}\right), \end{aligned} \tag{5}$$

where $A = [k_0(\varepsilon_k - p^2)]^{-1}$ and $Z_0 = (\mu_0/\epsilon_0)^{1/2}$ is the impedance of free space.

Azimuthal harmonics of the electric and magnetic fields inside the αth axon are described by the expressions

$$\begin{aligned} \begin{bmatrix} E_{z;\alpha,m} \\ H_{z;\alpha,m} \end{bmatrix} &= \begin{bmatrix} B_{\alpha,m}^{(1)} \\ Z_0^{-1}B_{\alpha,m}^{(2)} \end{bmatrix} q_3 J_m(k_0 q_3 \rho_\alpha), \quad \rho_\alpha \le a_1, \\ \begin{bmatrix} E_{z;\alpha,m} \\ H_{z;\alpha,m} \end{bmatrix} &= \sum_{k=1}^{2} \begin{bmatrix} C_{\alpha,m}^{(k)} \\ Z_0^{-1}\tilde{C}_{\alpha,m}^{(k)} \end{bmatrix} q_2 H_m^{(k)}(k_0 q_2 \rho_\alpha), \quad a_1 \le \rho_\alpha \le a_2, \end{aligned} \tag{6}$$

where $B_{\alpha,m}^{(1,2)}$, $C_{\alpha,m}^{(1,2)}$, and $\tilde{C}_{\alpha,m}^{(1,2)}$ are the amplitude coefficients corresponding to the mth azimuthal harmonic; J_m is the Bessel function of the first kind of order m; and $H_m^{(1)}$ and $H_m^{(2)}$ are the mth-order Hankel functions of the first and second kinds, respectively.

In the outer medium, the field outside the αth axon can be represented as a superposition of the field scattered by this axon and the field incident on it from axons with the numbers $\beta \neq \alpha$. Such a representation in terms of the scattered and incident fields provides a relatively simple way to solve the problem of determining the field of a particular eigenmode on a nerve fiber.

Azimuthal harmonics of the electric and magnetic fields scattered by the αth axon are represented in its coordinate system in the form

$$\begin{bmatrix} E_{z;\alpha,m}^{(\rm sc)} \\ H_{z;\alpha,m}^{(\rm sc)} \end{bmatrix} = \begin{bmatrix} D_{\alpha,m}^{(1)} \\ Z_0^{-1}D_{\alpha,m}^{(2)} \end{bmatrix} q_1 H_m^{(2)}(k_0 q_1 \rho_\alpha), \tag{7}$$

where $D^{(1)}_{\alpha,m}$ and $D^{(2)}_{\alpha,m}$ are the scattering coefficients corresponding to the azimuthal index m. To determine these coefficients, we represent the total field in the outer medium using a coordinate system of the αth axon. Employing Graf's addition theorem for cylindrical functions [27], we recalculate the azimuthal field harmonics at some observation point P [see Fig. 1(a)] from the coordinate system of the βth axon to that of the αth axon [27, 28]:

$$H^{(2)}_n\left(k_0 q_1 \rho_\beta\right)\exp(-in\phi_\beta) = \sum_{m=-\infty}^{\infty} J_m\left(k_0 q_1 \rho_\alpha\right) H^{(2)}_{m-n}\left(k_0 q_1 \rho_{\beta\alpha}\right)\exp\left[i(m-n)\phi_{\beta\alpha} - im\phi_\alpha\right]. \tag{8}$$

Here, $\phi_{\beta\alpha}$ is the azimuthal coordinate of the axis of the βth axon in the coordinate system of the αth axon, and $\rho_{\beta\alpha}$ is the distance between the axes of these axons. In Eq. (8), the condition $\rho_\alpha < \rho_{\beta\alpha}$ is assumed to be fulfilled, which is ensured by using Eq. (8) for representing the incident field only at the outer boundary of the axon. Then the azimuthal harmonics of the total field components outside the axons in the coordinate system of the αth axon take the form

$$E_{z;\alpha,m} = E^{(\mathrm{sc})}_{z;\alpha,m} + E^{(\mathrm{ex})}_{z;\alpha,m}, \quad H_{z;\alpha,m} = H^{(\mathrm{sc})}_{z;\alpha,m} + H^{(\mathrm{ex})}_{z;\alpha,m}, \tag{9}$$

where

$$E^{(\mathrm{ex})}_{z;\alpha,m} = q_1 \mathcal{E}_{\alpha,m} J_m\left(k_0 q_1 \rho_\alpha\right), \quad H^{(\mathrm{ex})}_{z;\alpha,m} = q_1 \mathcal{H}_{\alpha,m} J_m\left(k_0 q_1 \rho_\alpha\right).$$

Here,

$$\begin{bmatrix}\mathcal{E}_{\alpha,m}\\ \mathcal{H}_{\alpha,m}\end{bmatrix} = \sum_{\beta\neq\alpha}^{N_\mathrm{a}} \sum_{n=-\infty}^{\infty} \begin{bmatrix} D^{(1)}_{\beta,n} \\ Z_0^{-1} D^{(2)}_{\beta,n}\end{bmatrix} H^{(2)}_{m-n}\left(k_0 q_1 \rho_{\beta\alpha}\right)\exp\left[i(m-n)\phi_{\beta\alpha}\right], \tag{10}$$

where N_a is the total number of nerve fiber axons.

The coefficients $B^{(1,2)}_{\alpha,m}$, $C^{(1,2)}_{\alpha,m}$, $\tilde{C}^{(1,2)}_{\alpha,m}$, and $D^{(1,2)}_{\alpha,m}$ are determined using the boundary conditions for the tangential field components at the outer and inner surfaces of the myelin sheath of each axon. Based on the scattering matrix method [28], which is commonly employed for solving wave propagation problems in photonic crystals [29, 30], and making use of the boundary conditions at $\rho_\alpha = a_1$ and $\rho_\alpha = a_2$ for the αth axon, we arrive at the following system of equations for the coefficients $D^{(1)}_{\alpha,m}$ and $D^{(2)}_{\alpha,m}$:

$$D^{(1)}_{\alpha,m} = S^{ee}_m \mathcal{E}_{\alpha,m} + S^{eh}_m \mathcal{H}_{\alpha,m}, \quad D^{(2)}_{\alpha,m} = S^{he}_m \mathcal{E}_{\alpha,m} + S^{hh}_m \mathcal{H}_{\alpha,m}, \tag{11}$$

where S^{ee}_m, S^{eh}_m, S^{he}_m, and S^{hh}_m are the scattering-matrix elements for a single axon (see the appendix).

The application of Eq. (11) to each axon for the azimuthal indices $|m| \le M$ gives a system of $2N_\mathrm{a}(2M+1)$ homogeneous equations for the scattering coefficients $D^{(1)}_{\alpha,m}$ and $D^{(2)}_{\alpha,m}$, where M is the number of the highest-order azimuthal harmonic taken into account in the calculations. The summation over n in Eq. (10) is performed from $-M$ to M. The choice of the value of M is determined by the specified calculation accuracy. A dispersion relation which allows us to obtain the longitudinal wave numbers p of eigenmodes supported by the nerve fiber follows from the requirement that the determinant of this system is zero. The longitudinal wave numbers can be found as roots of the dispersion relation and are written as $p = p' - ip''$ for a lossy medium. Here, p' and p'' are the propagation and the attenuation constants, respectively. It will be ascertained in what follows that the quantity p'' is determined predominantly by the imaginary part of ε_w.

To obtain the field structure of the mode with the known longitudinal wave number p, one of the coefficients $D^{(1)}_{\alpha,m}$ and $D^{(2)}_{\alpha,m}$ can be chosen arbitrarily without loss of generality. The subscripts and superscript of such a coefficient will be denoted with a tilde below. For definiteness, we put the coefficient $D^{(\tilde{k})}_{\tilde{\alpha},\tilde{m}}$ equal to unity and choose the values of $\tilde{k}$, $\tilde{\alpha}$, and $\tilde{m}$ arbitrarily. This procedure yields the system of $2N_\mathrm{a}(2M+1)-1$ inhomogeneous linear equations for the coefficients $D^{(1)}_{\alpha,m}$ and $D^{(2)}_{\alpha,m}$, excepting $D^{(\tilde{k})}_{\tilde{\alpha},\tilde{m}}$. The right-hand sides of the equations of this linear system are formed with elements that are multiplied by the coefficient $D^{(\tilde{k})}_{\tilde{\alpha},\tilde{m}}$. Note that certain modes with different field structures can correspond to the same quantity p. The number of such different field structures for the same p value determines the degree of degeneracy of the corresponding eigenmodes.

In the case of a nerve consisting of a single axon, the system of linear equations is simplified to independent systems of linear equations. Each of such systems corresponds to a certain azimuthal index. Thus, a particular eigenmode of a single axon is characterized by a certain azimuthal number m and a radial index n, which is determined by the number of field oscillations along the radial coordinate (see, e.g., [31]).

3. DISPERSION PROPERTIES OF MODES

We now discuss dispersion properties of the eigenmodes guided by both a single axon and a nerve fiber consisting of three tightly packed axons. The effective dielectric permittivity of myelin is mainly determined by the sizes and dielectric properties of its molecular structures. For calculations, we use the following values of the characteristic parameters of the myelin sheath: $D_{\mathrm{B}} = 4.5\,\mathrm{nm}$, $D_{\mathrm{p}} = 1\,\mathrm{nm}$, $D_{\mathrm{I}} = 1\,\mathrm{nm}$, $D_{\mathrm{O}} = 3.5\,\mathrm{nm}$, $a_1 = 1.5\,\mu\mathrm{m}$, and $a_2 = 2.5\,\mu\mathrm{m}$. We consider two cases where the permittivity of myelin is determined by the values $\varepsilon_{\mathrm{lc}} = 3$ and $\varepsilon_{\mathrm{p}} = 4$ or $\varepsilon_{\mathrm{lc}} = 2$ and $\varepsilon_{\mathrm{p}} = 3$. To specify the maximum number $2M + 1$ of the azimuthal harmonics that are taken into account, we used the value $M = 5$ in all calculations.

To show numerical results, we will present the longitudinal wave numbers p of eigenmodes as functions of the free-space wavelength, which is given as $\lambda = 2\pi c/\omega$, where c is the speed of light in free space.

Figure 2 shows the dependences $p'(\lambda)$ and $\log p''(\lambda)$ for eigenmodes with the azimuthal indices $m = 0, 1, 2$, and 3 of a single axon for different values of the quantities $\varepsilon_{\mathrm{lc}}$ and ε_{p}. Namely, Figs. 2(a) and 2(b) present $p'(\lambda)$ and $\log p''(\lambda)$, respectively, for $\varepsilon_{\mathrm{lc}} = 3$ and $\varepsilon_{\mathrm{p}} = 4$, whereas Figs. 2(c) and 2(d) show the behavior of the respective quantities for $\varepsilon_{\mathrm{lc}} = 2$ and $\varepsilon_{\mathrm{p}} = 3$. We note that the propagation constant of each localized mode lies in the interval $P'_{\min} < p' < P'_{\max}$, where $P'_{\min} = \mathrm{Re}\sqrt{\varepsilon_{\mathrm{w}}}$ and

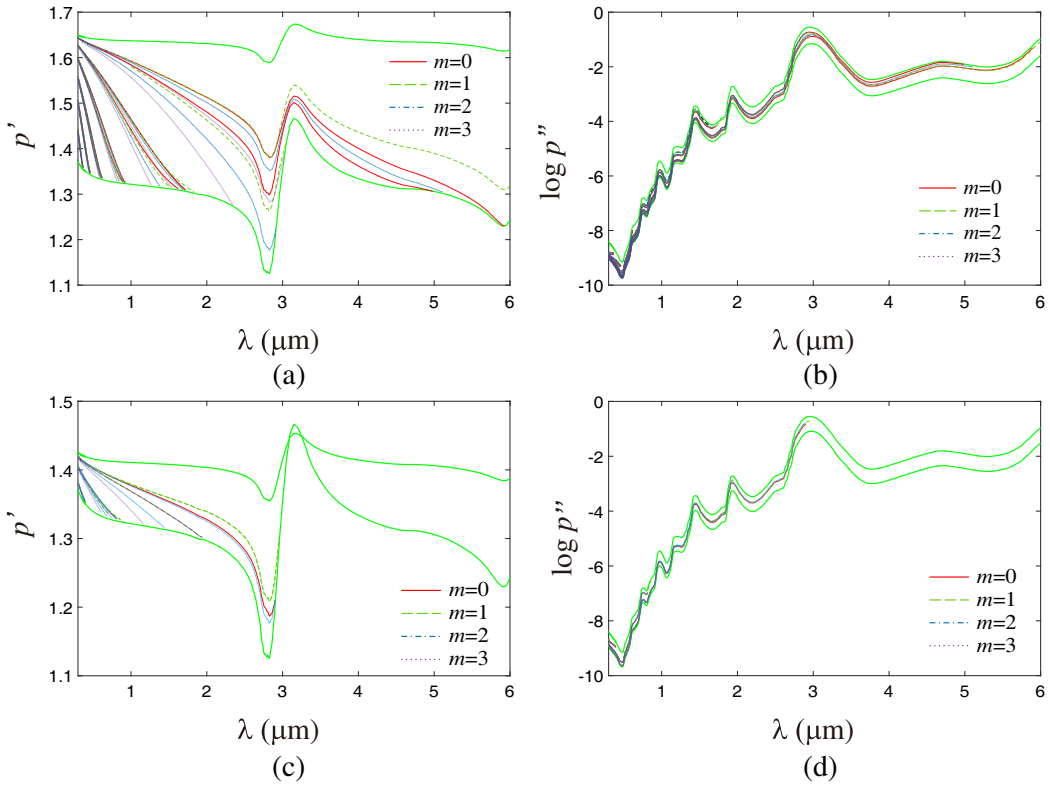

Figure 2. Dispersion curves of the single-axon eigenmodes with the azimuthal indices $m = 0$, 1, 2, and 3. Dependences (a) $p'(\lambda)$ and (b) $p''(\lambda)$ for $\varepsilon_{\mathrm{lc}} = 3$ and $\varepsilon_{\mathrm{p}} = 4$ and dependences (c) $p'(\lambda)$ and (d) $p''(\lambda)$ for $\varepsilon_{\mathrm{lc}} = 2$ and $\varepsilon_{\mathrm{p}} = 3$.

$P'_{\max} = \mathrm{Re}\sqrt{\varepsilon_2}$ are shown as functions of λ by the solid green lines in Figs. 2(a) and 2(c) and similar figures onwards. As the wavelength decreases to the low boundary of the optical range, the higher-order eigenmodes appear. With increasing wavelength, the curves $p'(\lambda)$ for the higher-order eigenmodes reach the lower boundary $P'_{\min}$, and the corresponding modes cease to exist. As a result, only the lowest dipole eigenmode with $m = 1$ remains to exist for relatively long wavelengths, up to the infrared range. Although nonsymmetric waves with $m = 1$ can exist in a wide wavelength interval, they have not received sufficient attention in previous works [18–21], in which the propagation of axisymmetric eigenmodes of a single axon was mostly considered.

In the wavelength range from 2.9 μm to 3.1 μm, some eigenmodes can be backward. For such waves, the directions of energy flow and wavefront propagation are opposite. These eigenmodes can be readily found in Figs. 2(a) and 2(c) if we take into account that their group velocity $v_g = c(p' + \omega\partial p'/\partial\omega)^{-1}$ is negative for positive p'.

It can be seen in Figs. 2(a) and 2(c) that the dispersion curves form separate groups, which include modes with different azimuthal indices and the same radial indices. This is especially evident at smaller values of λ. The modes of each group are divided into pairs such that the modes of a particular pair have the same azimuthal index but different polarizations (for example, in Fig. 2(a) there are eight modes in each group). In each pair for $m \neq 0$, the field of one mode is predominantly determined by the longitudinal magnetic-field component (HE modes), whereas the field of the other mode, by the longitudinal electric-field component (EH modes).

The attenuation constants of the single-axon eigenmodes are shown in Figs. 2(b) and 2(d). As expected, the values of these quantities lie in the interval $P''_{\min} < p'' < P''_{\max}$, where the quantities $P''_{\min} = -\mathrm{Im}\sqrt{\varepsilon_2} > 0$ and $P''_{\max} = -\mathrm{Im}\sqrt{\varepsilon_{\mathrm{w}}} > 0$ are determined by the imaginary parts of the dielectric

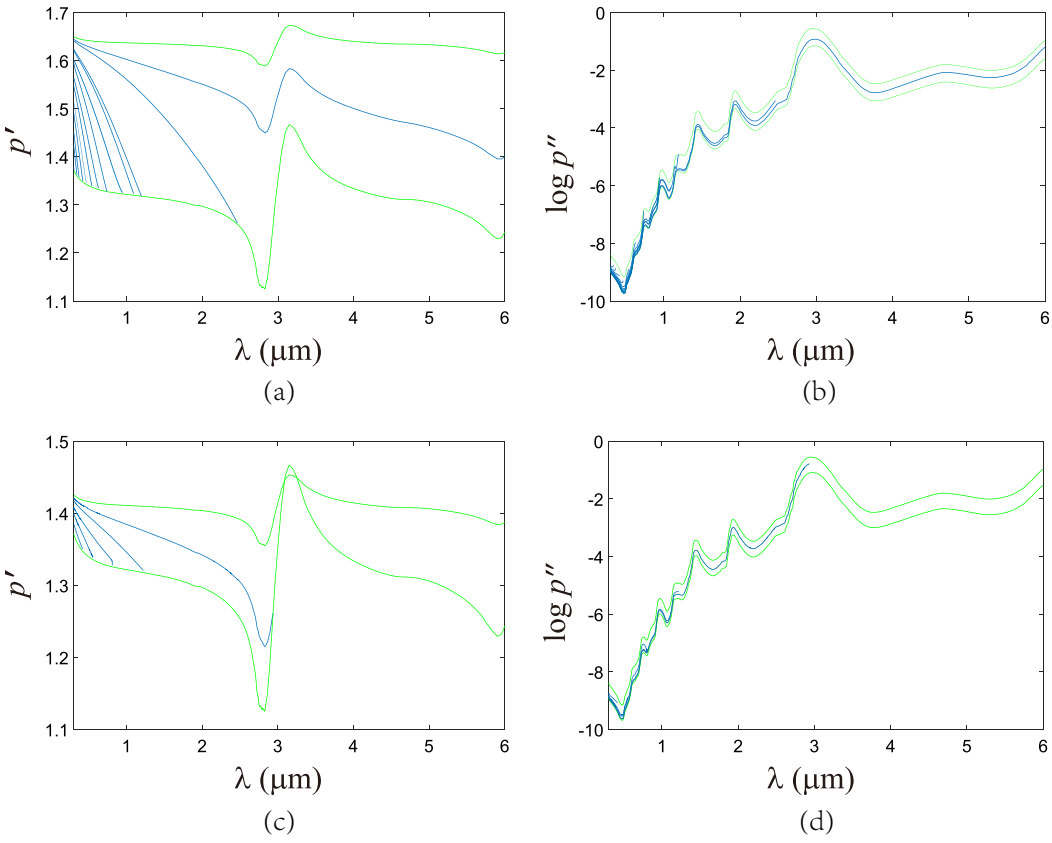

Figure 3. Dispersion curves of the eigenmodes of a nerve fiber consisting of three axons. Dependences (a) $p'(\lambda)$ and (b) $p''(\lambda)$ for $\varepsilon_{\mathrm{lc}} = 3$ and $\varepsilon_{\mathrm{p}} = 4$ and dependences (c) $p'(\lambda)$ and (d) $p''(\lambda)$ for $\varepsilon_{\mathrm{lc}} = 2$ and $\varepsilon_{\mathrm{p}} = 3$.

permittivities of myelin and water, respectively. The quantities $P''_{\min}$ and $P''_{\max}$ as functions of the wavelength λ are also indicated by the solid green lines in the figures. Note that in almost the entire wavelength range presented in the figures, the eigenmodes are weakly attenuated, except for local maxima of $p''(\lambda)$ corresponding to the frequencies of water resonance absorption. The maximum absorption takes place at $\lambda \simeq 3\,\mu$m.

It is worth noting that for a smaller optical density of myelin, when $\varepsilon_{\rm lc} = 2$ and $\varepsilon_{\rm p} = 3$, attenuation of the modes propagating along the axon [see Fig. 2(d)] is somewhat greater because of a weaker localization of their fields. It has also been found numerically that the lowest nonsymmetric eigenmode turns out to be propagating at shorter wavelengths than those for the optically denser myelin considered above.

Figure 3 shows the dependences $p'(\lambda)$ and $p''(\lambda)$ for eigenmodes of a nerve fiber consisting of three tightly packed axons for the previously chosen values of $\varepsilon_{\rm lc}$ and $\varepsilon_{\rm p}$. The dispersion curves of the modes of such a nerve fiber differ significantly from those for the modes of a single axon. This is especially clearly seen when comparing the dispersion curves of the lowest modes of a single axon and a nerve fiber. In addition, the number of the dispersion curves for modes of a nerve fiber is less than that for an axon. This can be explained by degeneracy or near-degeneracy of some modes of the fiber. For example, the dispersion curves of the two different lowest eigenmodes are located so closely in Figs 3(a) and 3(b) that they cannot be seen as separate ones. Therefore, the total number of modes supported by the nerve fiber is actually no less than that of modes supported by individual axons.

The presented results also demonstrate that the dependences $p'(\lambda)$ and $p''(\lambda)$ for eigenmodes of a nerve fiber consisting of tightly packed axons are fairly sensitive to variations in the values of the parameters $\varepsilon_{\rm lc}$ and $\varepsilon_{\rm p}$. For example, the behavior of the dispersion curves and their total number in Figs. 3(c) and 3(d), which are plotted for $\varepsilon_{\rm lc} = 2$ and $\varepsilon_{\rm p} = 3$, differ significantly from those in the case presented in Figs. 3(a) and 3(b) for $\varepsilon_{\rm lc} = 3$ and $\varepsilon_{\rm p} = 4$.

4. FIELD STRUCTURES OF MODES

Let us analyze the eigenmode fields for a single axon and the nerve fiber. To this end, we present the spatial distributions of these fields in relative units. Figs. 4, 5, and 6 show the distributions of the longitudinal electric and magnetic fields in the eigenmodes of a singe axon at $\lambda = 1\,\mu$m for $m = 0$, $m = 1$, and $m = 2$, respectively. It can be seen that the fields of these modes are concentrated mainly near the inner and outer boundaries of the myelin sheath of the axon. The number of the field oscillations along the azimuthal coordinate increases with increasing azimuthal index of the mode. All these modes belong to the same group, which is characterized by the lowest number ($n = 1$) of the field oscillations along the radial coordinate. Note that the field structures of eigenmodes with azimuthal indices $m = 0$ and $m = 1$ in Figs. 4 and 5, respectively, are in agreement with the results reported earlier by other authors for such modes [18–21].

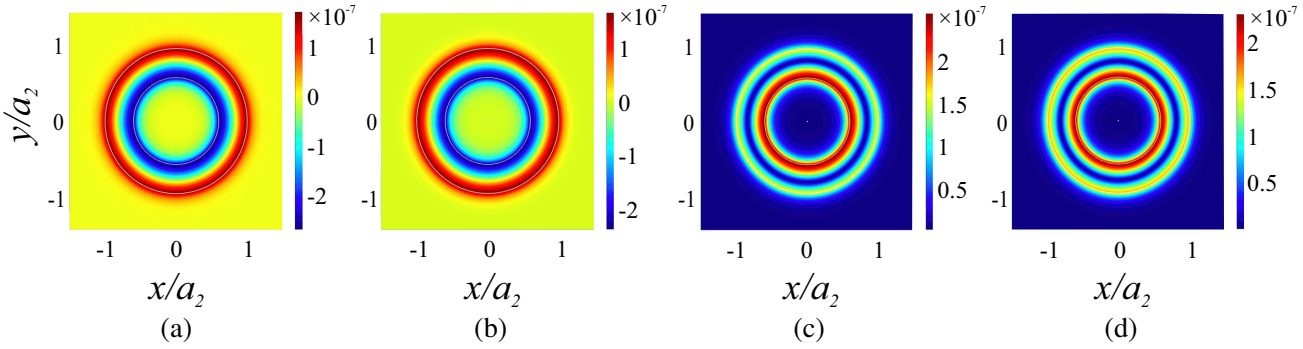

Figure 4. Snapshots of the (a) E_z and (b) H_z components in the axisymmetric E and H eigenmodes of a single axon at $\lambda = 1\,\mu$m, with $p = 1.5926 - i8.761 \times 10^{-7}$ and $p = 1.5927 - i8.76 \times 10^{-7}$, respectively, and the distributions of the corresponding magnitudes (c) $|E_z|$ and (d) $|H_z|$ for $\varepsilon_{\rm lc} = 3$ and $\varepsilon_{\rm p} = 4$.

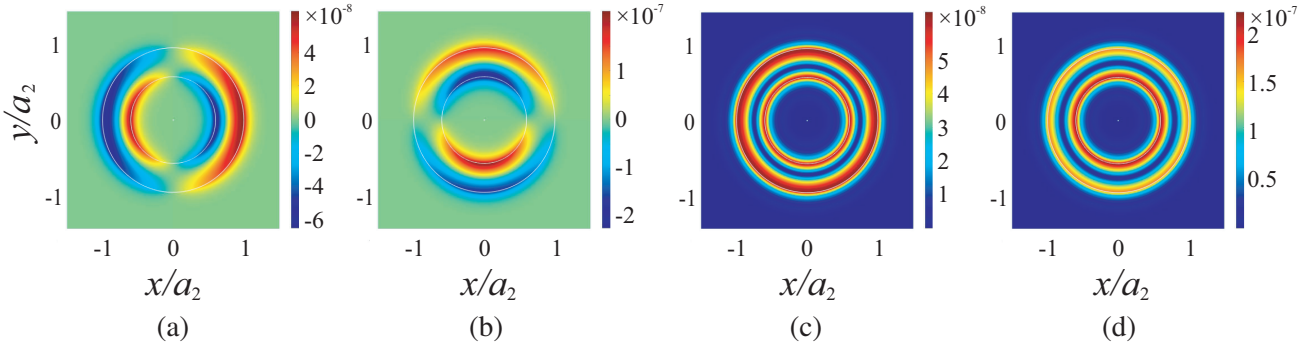

Figure 5. Snapshots of the (a) E_z and (b) H_z components in the $m = 1$ HE eigenmode of a single axon at $\lambda = 1\,\mu$m, with $p = 1.592 - i8.86 \times 10^{-7}$, and the distributions of the corresponding magnitudes (c) $|E_z|$ and (d) $|H_z|$. Same parameters as in Fig. 4.

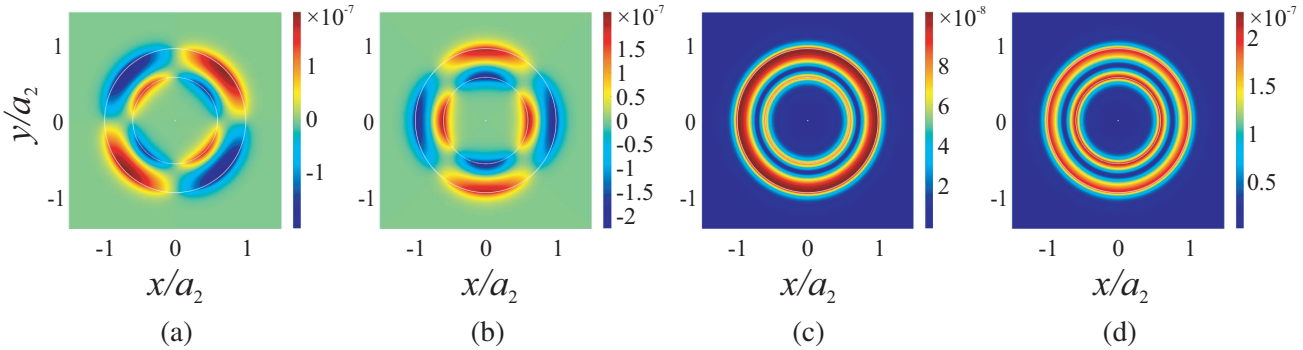

Figure 6. Snapshots of the (a) E_z and (b) H_z components in the $m = 2$ HE eigenmode of a single axon at $\lambda = 1\,\mu$m, with $p = 1.59 - i8.95 \times 10^{-7}$, and the distributions of the corresponding magnitudes (c) $|E_z|$ and (d) $|H_z|$. Same parameters as in Fig. 4.

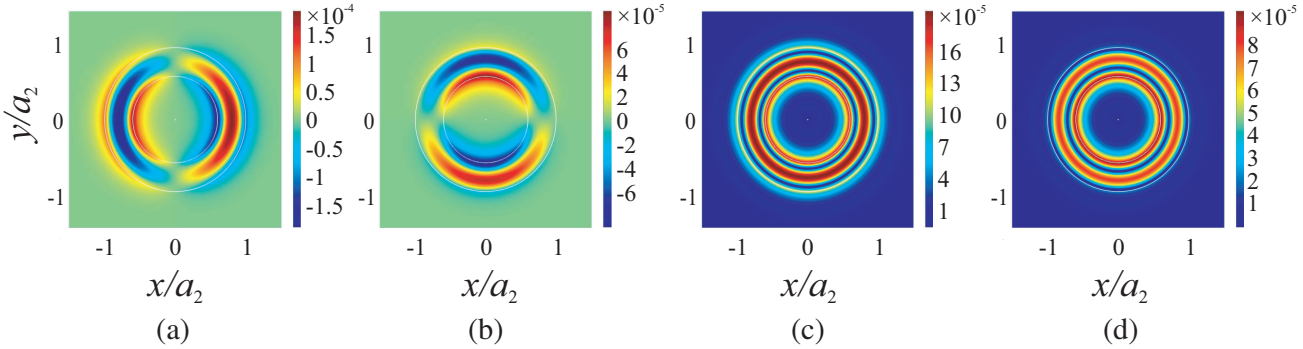

Figure 7. Snapshots of the (a) E_z and (b) H_z components in the $m = 1$ EH eigenmode of a single axon at $\lambda = 1\,\mu$m, with $p = 1.439 - i1.53 \times 10^{-6}$ and $n = 2$, and the distributions of the corresponding magnitudes (c) $|E_z|$ and (d) $|H_z|$. Same parameters as in Fig. 4.

It follows from the numerical calculations that at the given value of λ, the modes with greater propagation constants have smaller attenuation constants. This can be explained by the fact that the fields of modes with the higher propagation constants are predominantly localized in the myelin sheath, which is characterized by a weaker absorption of electromagnetic energy. To illustrate this fact, the field structure of the $m = 1$ eigenmode with the radial index $n = 2$ is presented in Fig. 7 for the comparison with Fig. 5.

Figure 8 shows the field distributions of the lowest mode of the above-described nerve fiber at $\lambda = 1\,\mu\text{m}$. It is clearly seen that the field of this mode, which has the highest propagation constant at the chosen value of λ, is characterized by the third-order rotational symmetry. Note that a similar field structure obtained by the mutual replacement of the electric and magnetic fields (see Fig. 9) is observed in a mode with the propagation constant that is close to the propagation constant of the mode whose field is shown in Fig. 8.

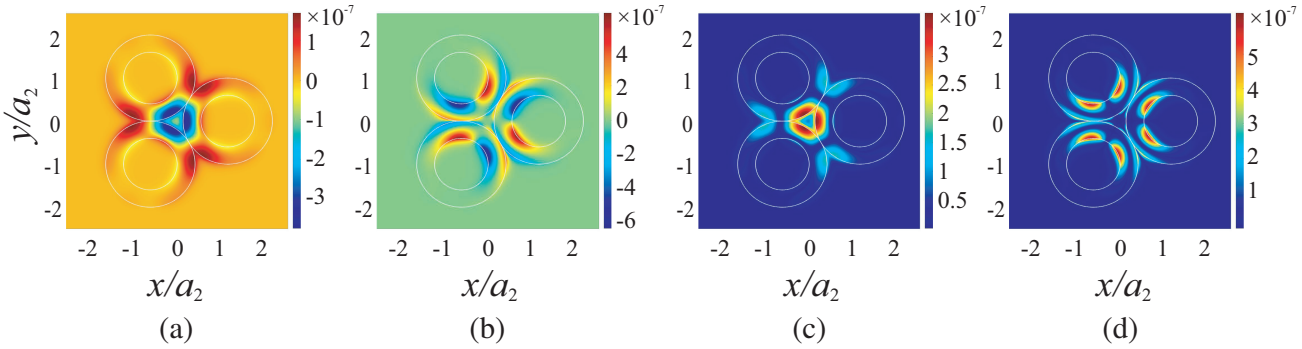

Figure 8. Snapshots of the (a) E_z and (b) H_z components in the rotationally symmetric hybrid eigenmode of a nerve fiber at $\lambda = 1\,\mu\text{m}$, with $p = 1.6 - i8.46 \times 10^{-7}$, and the distributions of the corresponding magnitudes (c) $|E_z|$ and (d) $|H_z|$. Same parameters as in Fig. 4.

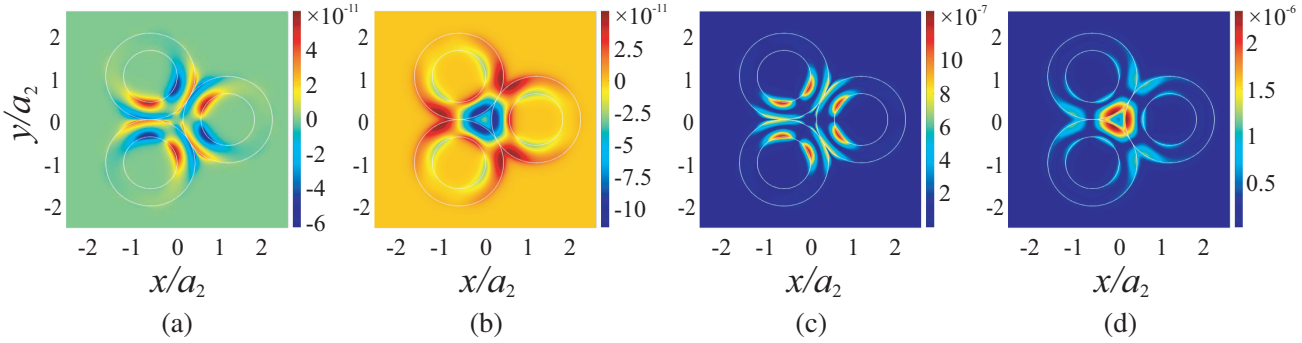

Figure 9. Snapshots of the (a) E_z and (b) H_z components in the rotationally symmetric hybrid eigenmode of a nerve fiber at $\lambda = 1\,\mu\text{m}$, with $p = 1.596 - i8.93 \times 10^{-7}$, and the distributions of the corresponding magnitudes (c) $|E_z|$ and (d) $|H_z|$. Same parameters as in Fig. 4.

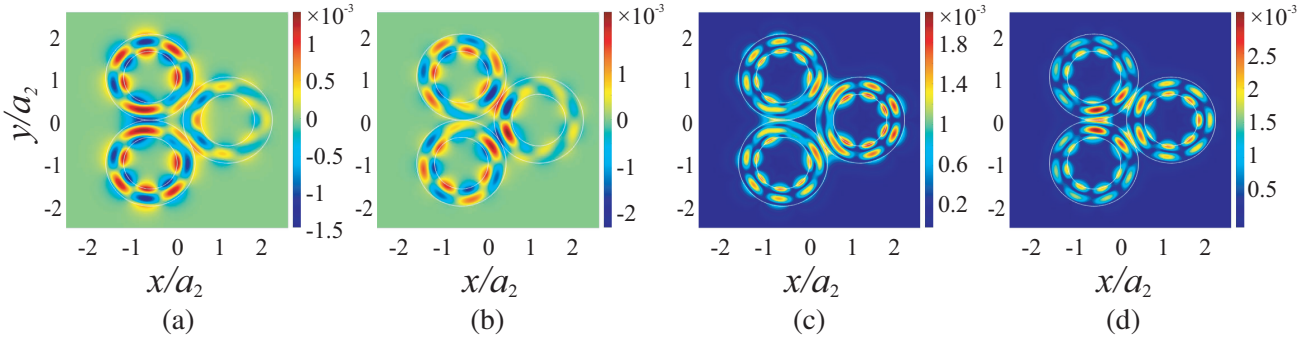

Figure 10. Snapshots of the (a) E_z and (b) H_z components in the rotationally nonsymmetric hybrid eigenmode of a nerve fiber at $\lambda = 1\,\mu\text{m}$, with $p = 1.395 - i1.39 \times 10^{-6}$, and the distributions of the corresponding magnitudes (c) $|E_z|$ and (d) $|H_z|$. Same parameters as in Fig. 4.

In addition to the modes with rotational symmetry, the nerve fiber can support the propagation of waves lacking this symmetry. Figs. 10 and 11 show the structures of the electric and magnetic fields of two such modes, which are degenerate, i.e., have identical longitudinal wave numbers but different field structures. Note that the field distributions in Fig. 11 can be obtained from those in Fig. 10 by rotation by 120 degrees relative to the symmetry axis of the nerve fiber.

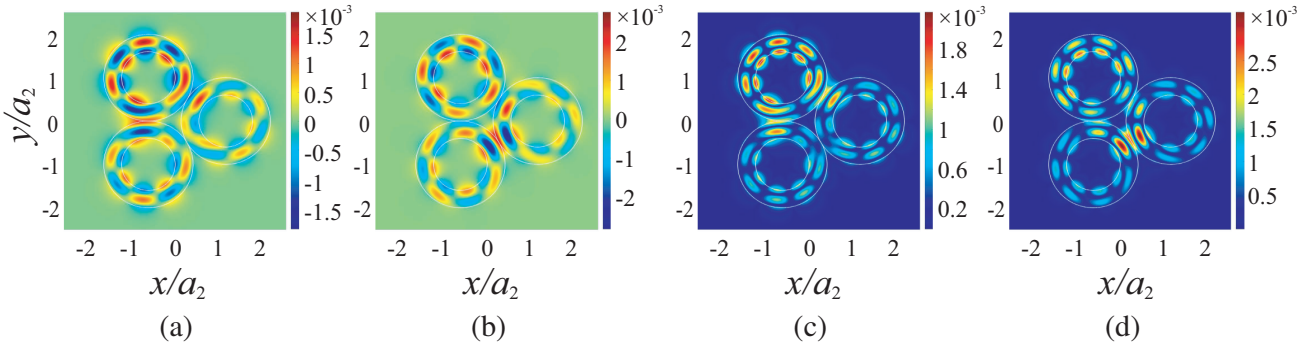

Figure 11. Snapshots of the (a) E_z and (b) H_z components in the rotationally nonsymmetric hybrid eigenmode of a nerve at $\lambda = 1\,\mu\text{m}$, with $p = 1.395 - i1.39 \times 10^{-6}$, and the distributions of the corresponding magnitudes (c) $|E_z|$ and (d) $|H_z|$. The mode shown in this figure is degenerate with that presented in Fig. 10. Same parameters as in Fig. 4.

It is also worth mentioning that the results obtained for a nerve fiber consisting of three axons were verified by increasing the distance between the axons. In this case, the field distributions and dispersion characteristics of the fiber modes gradually transformed to those of individual axons, as expected. We do not present the corresponding results here for the sake of brevity.

5. CONCLUSION

In this work, the properties of the guided propagation of electromagnetic waves along a single idealized myelinated axon and a nerve fiber consisting of such axons have been studied in the optical and infrared ranges. The fundamental possibility of the existence of localized, weakly attenuated modes in structures of this type has been demonstrated. Frequency dependences of the propagation and attenuation constants of eigenmodes supported by both a single axon and a nerve fiber, as well as their field structures, have been found numerically for the indicated ranges. It is confirmed that the propagation constants of the eigenmodes lie between the refractive indices of the media in the outer and myelin regions of the axons. Modes with larger propagation constants were found to have smaller attenuation constants due to better localization of their fields in the myelin sheath. This can be explained by the weak energy absorption in myelin compared with the outer and inner media, which consist predominantly of water. It has also been established numerically that when the optical density of the myelin decreases, the dispersion properties of eigenmodes do not change significantly, but this leads to a decrease in the number of modes supported by the nerve fiber. Moreover, the differences between the dispersion properties and field structures of the eigenmodes guided by the considered nerve fiber and a single axon have been revealed. It has been shown that the nerve fiber supports the guided propagation of modes that have rotational symmetry and modes that have no such symmetry. The latter, in turn, form sets of modes with polarization degeneracy.

The results obtained may be useful in the development of new contactless methods for stimulating nerve fibers and application of electromagnetic waves guided by a set of axons as a part of the mechanism of a cell-to-cell communication. The approach of this work can also be extended to the case where the nerve fiber is stimulated by a nonmonochromatic signal. Future work should be primarily focused on studying the excitation of electromagnetic waves by given sources, both monochromatic and nonmonochromatic, in the presence of a nerve fiber, along with the analysis of the wave propagation in a nerve fiber that consists of myelinated axons with periodic gaps in the myelin sheath.

ACKNOWLEDGMENT

This work was supported by the Ministry of Science and Higher Education of the Russian Federation (project No. FSWR-2023-0031).

APPENDIX A. OBTAINING THE SCATTERING MATRIX OF A SINGLE MYELINATED AXON

If a cylindrical wave with the azimuthal index m is incident on a single axon, the coefficients of the field are found from a system of linear equations which are derived using the boundary conditions at $\rho_\alpha = a_1$ and $\rho_\alpha = a_2$. In matrix form, this system of equations is written as follows:

$$\begin{pmatrix} \hat{J}_m & 0 & -\hat{H}_{m,1}^{(1)} & -\hat{H}_{m,1}^{(2)} & 0 & 0 & 0 & 0 \\ 0 & \hat{J}_m & 0 & 0 & -\hat{H}_{m,1}^{(1)} & -\hat{H}_{m,1}^{(2)} & 0 & 0 \\ -\tilde{J}_m & \mathring{J}_m & \tilde{H}_{m,1}^{(1)} & \tilde{H}_{m,1}^{(2)} & -\mathring{H}_{m,1}^{(1)} & -\mathring{H}_{m,1}^{(2)} & 0 & 0 \\ -\varepsilon_3\mathring{J}_m & -\tilde{J}_m & \varepsilon_2\mathring{H}_{m,1}^{(1)} & \varepsilon_2\mathring{H}_{m,1}^{(2)} & \tilde{H}_m^{(1)} & \tilde{H}_{m,1}^{(2)} & 0 & 0 \\ 0 & 0 & -\hat{H}_{m,2}^{(1)} & -\hat{H}_{m,2}^{(2)} & 0 & 0 & \hat{H}_m^{(2)} & 0 \\ 0 & 0 & 0 & 0 & -\hat{H}_{m,2}^{(1)} & -\hat{H}_{m,2}^{(2)} & 0 & \hat{H}_m^{(2)} \\ 0 & 0 & \tilde{H}_{m,2}^{(1)} & \tilde{H}_{m,2}^{(2)} & -\mathring{H}_{m,2}^{(1)} & -\mathring{H}_{m,2}^{(2)} & -\tilde{H}_m^{(2)} & \mathring{H}_m^{(2)} \\ 0 & 0 & \varepsilon_2\mathring{H}_{m,2}^{(1)} & \varepsilon_2\mathring{H}_{m,2}^{(2)} & \tilde{H}_{m,2}^{(1)} & \tilde{H}_{m,2}^{(2)} & -\varepsilon_1\mathring{H}_m^{(2)} & -\tilde{H}_m^{(2)} \end{pmatrix} \begin{pmatrix} \mathcal{B}_m^{(1)} \\ \mathcal{B}_m^{(2)} \\ \mathcal{C}_m^{(1)} \\ \mathcal{C}_m^{(2)} \\ \tilde{\mathcal{C}}_m^{(1)} \\ \tilde{\mathcal{C}}_m^{(2)} \\ \mathcal{D}_m^{(1)} \\ \mathcal{D}_m^{(2)} \end{pmatrix} = \mathcal{A}_m^{(1)}\mathbf{I}^{(1)} + \mathcal{A}_m^{(2)}\mathbf{I}^{(2)}, \tag{A1}$$

$$\mathbf{I}^{(1)} = \begin{pmatrix} 0 & 0 & 0 & 0 & -q_1 J_m(Q_1) & 0 & \dfrac{pm}{Q_1} J_m(Q_1) & i\varepsilon_1 J_m'(Q_1) \end{pmatrix}^{\mathrm{T}},$$

$$\mathbf{I}^{(2)} = \begin{pmatrix} 0 & 0 & 0 & 0 & 0 & -q_1 J_m(Q_1) & -iJ_m'(Q_1) & \dfrac{pm}{Q_1} J_m(Q_1) \end{pmatrix}^{\mathrm{T}}.$$

Here,

$$\begin{aligned} &\hat{J}_m = q_3 J_m(Q_3), \quad \hat{H}_{m,\gamma}^{(k)} = q_2 H_m^{(k)}(\tilde{Q}_\gamma), \quad \hat{H}_m^{(2)} = q_1 H_m^{(2)}(Q_1), \\ &\tilde{J}_m = \frac{pm}{Q_3} J_m(Q_3), \quad \tilde{H}_{m,\gamma}^{(k)} = \frac{pm}{\tilde{Q}_\gamma} H_m^{(k)}(\tilde{Q}_\gamma), \quad \tilde{H}_m^{(2)} = \frac{pm}{Q_1} H_m^{(2)}(Q_1), \\ &\mathring{J}_m = iJ_m'(Q_3), \quad \mathring{H}_{m,\gamma}^{(k)} = iH_m^{(k)\prime}(\tilde{Q}_\gamma), \quad \mathring{H}_m^{(2)} = iH_m^{(2)\prime}(Q_1), \end{aligned} \tag{A2}$$

where $\gamma = 1, 2$, $Q_1 = k_0 q_1 a_2$, $\tilde{Q}_\gamma = k_0 q_2 a_\gamma$, $Q_3 = k_0 q_3 a_1$, and the superscript T stands for the transposition operation. In Eq. (A1), the prime indicates the derivative with respect to the argument. Upon finding the field coefficients $\mathcal{B}_{\alpha,m}^{(1,2)}$, $\mathcal{C}_{\alpha,m}^{(1,2)}$, $\tilde{\mathcal{C}}_{\alpha,m}^{(1,2)}$, and $\mathcal{D}_{\alpha,m}^{(1,2)}$ from the system in Eq. (A1) with allowance for Eq. (A2), we represent the scattering-matrix elements S_m^{ee}, S_m^{he}, S_m^{eh}, and S_m^{hh} in Eq. (11) as $S_m^{ee} = \mathcal{D}_m^{(1)}$ and $S_m^{he} = \mathcal{D}_m^{(2)}$ under the conditions $\mathcal{A}_m^{(1)}$=1 and $\mathcal{A}_m^{(2)}$=0, and as $S_m^{eh} = \mathcal{D}_m^{(1)}$ and $S_m^{hh} = \mathcal{D}_m^{(2)}$ under the conditions $\mathcal{A}_m^{(1)}$=0 and $\mathcal{A}_m^{(2)}$=1.

REFERENCES

1. Musk, E., "An integrated brain-machine interface platform with thousands of channels," *J. Med. Internet Res.*, Vol. 21, No. 10, e16194, 2019.
2. Song, E., J. Li, S. M. Won, W. Bai, and J. A. Rogers, "Materials for flexible bioelectronic systems as chronic neural interfaces," *Nature Mater.*, Vol. 19, No. 6, 590–603, 2020.
3. Ayton, L. N., N. Barnes, G. Dagnelie, T. Fujikado, G. Goetz, R. Hornig, B. W. Jones, M. M. Muqit, D. L. Rathbun, K. Stingl, J. D. Weiland, and M. A. Petoe, "An update on retinal prostheses," *Clinical Neurophysiol.*, Vol. 131, No. 6, 1383–1398, 2020.

4. Plaksin, M., E. Kimmel, and S. Shoham, "Cell-type-selective effects of intramembrane cavitation as a unifying theoretical framework for ultrasonic neuromodulation," *eNeuro*, Vol. 3, No. 3, e0136-15.2016, 2016.
5. Basser, P. J. and B. J. Roth, "Stimulation of a myelinated nerve axon by electromagnetic induction," *Med. Biol. Eng. Comput.*, Vol. 29, No. 3, 261–268, 1991.
6. Fork, R. L., "Laser stimulation of nerve cells in aplysia," *Science*, Vol. 171, No. 3974, 907–908, 1971.
7. Abaya, T., S. Blair, P. Tathireddy, L. Rieth, and F. Solzbacher, "A 3D glass optrode array for optical neural stimulation," *Biomed. Opt. Express*, Vol. 3, No. 12, 3087–3104, 2012.
8. Ford, J. B., M. W. Jenkins, H. J. Chiel, and E. D. Jansen, "Reducing peak temperatures during infrared inhibition of neural potentials," *Optogenetics and Optical Manipulation, Proc. SPIE*, Vol. 10052, 28–34, 2017.
9. Shapiro, M. G., K. Homma, S. Villarreal, C.-P. Richter, and F. Bezanilla, "Infrared light excites cells by changing their electrical capacitance," *Nature Commun.*, Vol. 3, No. 1, 736–746, 2012.
10. Angotzi, G. N., F. Boi, A. Lecomte, E. Miele, M. Malerba, S. Zucca, A. Casile, and L. Berdondini, "SiNAPS: An implantable active pixel sensor CMOS-probe for simultaneous large-scale neural recordings," *Biosensors Bioelectron.*, Vol. 126, 355–364, 2019.
11. Leonard, J. T., D. A. Cohen, B. P. Yonkee, R. M. Farrell, T. Margalith, S. Lee, S. P. DenBaars, J. S. Speck, and S. Nakamura, "Nonpolar III-nitride vertical-cavity surface-emitting lasers incorporating an ion implanted aperture," *Appl. Phys. Lett.*, Vol. 107, No. 1, 011102, 2015.
12. Marblestone, A. H., B. M. Zamft, Y. G. Maguire, M. G. Shapiro, T. R. Cybulski, J. I. Glaser, D. Amodei, P. B. Stranges, R. Kalhor, D. A. Dalrymple, D. Seo, E. Alon, M. M. Maharbiz, J. M. Carmena, J. M. Rabaey, E. S. Boyden, G. M. Church, and K. P. Kording, "Physical principles for scalable neural recording," *Frontiers Comput. Neurosci.*, Vol. 7, 137, 2013.
13. Zhou, R., Z. Mou, D. Yang, and X. Wang, "Theoretical simulation of the selective stimulation of axons in different areas of a nerve bundle by multichannel near-infrared lasers," *Med. Biol. Eng. Comput.*, Vol. 60, No. 1, 205–220, 2022.
14. Chernov, M. M., R. M. Friedman, and A. W. Roe, "Fiberoptic array for multiple channel infrared neural stimulation of the brain," *Neurophotonics*, Vol. 8, No. 2, 025005, 2021.
15. Zhu, X., J.-W. Lin, A. Turnali, and M. Y. Sander, "Single infrared light pulses induce excitatory and inhibitory neuromodulation," *Biomed. Opt. Express*, Vol. 13, No. 1, 374–388, 2022.
16. Es'kin, V. A., A. V. Kudrin, and A. A. Popova, "Excitation of an electromagnetic field in a compact nerve fiber by a system of filamentary electric currents," *Radiophys. Quantum Electron.*, Vol. 62, No. 1, 65–76, 2019.
17. Es'kin, V. A., A. V. Kudrin, and A. A. Popova, "Excitation of an electromagnetic field in a large nerve fiber by an array of electric-dipole filaments," *2020 XXXIIIrd General Assembly and Scientific Symposium of the International Union of Radio Science*, 1–4, Rome, Italy, August 29–September 5, 2020.
18. Kumar, S., K. Boone, J. Tuszyński, P. Barclay, and C. Simon, "Possible existence of optical communication channels in the brain," *Sci. Rep.*, Vol. 6, 36508, 2016.
19. Zangari, A., D. Micheli, R. Galeazzi, and A. Tozzi, "Node of Ranvier as an array of bio-nanoantennas for infrared communication in nerve tissue," *Sci. Rep.*, Vol. 8, 539, 2018.
20. Liu, G., C. Chang, Z. Qiao, K. Wu, Z. Zhu, G. Cui, W. Peng, Y. Tang, J. Li, and C. Fan, "Myelin sheath as a dielectric waveguide for signal propagation in the mid-infrared to terahertz spectral range," *Adv. Funct. Mater.*, Vol. 29, No. 7, 1807862, 2019.
21. Maghoul, A., A. Khaleghi, and I. Balasingham, "Engineering photonic transmission inside brain nerve fibers," *IEEE Access*, Vol. 9, 35399–35410, 2021.
22. Xiang, Z., C. Tang, C. Chang, and G. Liu, "A primary model of THz and far-infrared signal generation and conduction in neuron systems based on the hypothesis of the ordered phase of water molecules on the neuron surface I: Signal characteristics," *Sci. Bull.*, Vol. 65, No. 4, 308–317, 2020.

23. Xiang, Z., C. Tang, C. Chang, and G. Liu, "A new viewpoint and model of neural signal generation and transmission: Signal transmission on unmyelinated neurons," *Nano Res.*, Vol. 14, No. 3, 590–600, 2021.
24. Segelstein, D. J., "The complex refractive index of water," M.Sc. thesis, University of Missouri, 1981.
25. Min, Y., K. Kristiansen, J. M. Boggs, C. Husted, J. A. Zasadzinski, and J. Israelachvili, "Interaction forces and adhesion of supported myelin lipid bilayers modulated by myelin basic protein," *Proc. Natl. Acad. Sci. USA*, Vol. 106, No. 9, 3154–3159, 2009.
26. Bioud, F.-Z., P. Gasecka, P. Ferrand, H. Rigneault, J. Duboisset, and S. Brasselet, "Structure of molecular packing probed by polarization-resolved nonlinear four-wave mixing and coherent anti-Stokes Raman-scattering microscopy," *Phys. Rev. A*, Vol. 89, No. 1, 013836, 2014.
27. Abramowitz, M. and I. A. Stegun, eds., *Handbook of Mathematical Functions, with Formulas, Graphs, and Mathematical Tables*, Dover, Mineola, 1974.
28. Yasumoto, K., *Electromagnetic Theory and Applications for Photonic Crystals*, Taylor and Francis, Boca Raton, 2006.
29. Vendromin, C. and M. M. Dignam, "Simple way to incorporate loss when modeling multimode-entangled-state generation," *Phys. Rev. A*, Vol. 105, No. 6, 063707, 2022.
30. Kocharovsky, V. V., C. B. Reynolds, and Vl. V. Kocharovsky, "Eigenmodes of a lamellar optical grating: Profile, propagation, reflection, transmission, and nonadiabatic mode coupling," *Phys. Rev. A*, Vol. 100, No. 5, 053854, 2019.
31. Ostafiychuk, O. M., V. A. Es'kin, A. V. Kudrin, and A. A. Popova, "Electromagnetic waves guided by a myelinated axon in the optical and infrared ranges," *2019 Photonics & Electromagnetics Research Symposium — Spring (PIERS — Spring)*, 1180–1184, Rome, Italy, June 17–20, 2019.